Appl Nanosci (2012) 2:203–210
DOI 10.1007/s13204-012-0084-x

ORIGINAL ARTICLE

Electromagnetic properties of microwave sintered $xTiO_2 + (1 - x)\ CoFe_2O_4$ nanocomposites

K. Sadhana · K. Praveena · P. Raju · S. R. Murthy

Received: 22 November 2011 / Accepted: 6 March 2012 / Published online: 30 March 2012

Abstract The nanocomposites of $xTiO_2 + (1 - x)\ CoFe_2O_4$ (where $0 \leq x \geq 1$) were prepared using microwave–hydrothermal method at 165 °C/45 min. The as-synthesized powders were characterized using X-ray diffraction (XRD), transmission electron microscope and Fourier transform infrared spectroscopy. The particle size was found to be ~18, ~22 and 24 nm for TiO_2, $CoFe_2O_4$, 50 mol% TiO_2 + 50 mol% $CoFe_2O_4$ composite powder, respectively. The as-prepared powders were densified at 500 °C/30 min using microwave sintering method. The sintered composite samples were characterized using XRD and field emission scanning electron microscopy. The bulk densities of the present composites were increasing with an addition of TiO_2. The saturation magnetization of composites decreased with an increase of TiO_2 content. The grain sizes of all the composite lies between 54 and 78 nm. The addition of TiO_2 to ferrite increased ε' and ε'' and the resonant frequency of all the sintered samples were found to be >1 GHz. The value of μ'' found to increase with an increase of TiO_2.

Keywords Microwave sintering · Dielectric properties · Magnetic properties

K. Sadhana · K. Praveena · P. Raju · S. R. Murthy
Department of Physics, Osmania University,
Hyderabad 500 007, India

Present Address:
K. Sadhana (✉)
Materials Research Centre, Indian Institute of Science,
Bangalore 560012, India
e-mail: sadhanaphysics@gmail.com

Present Address:
K. Praveena
School of Physics, University of Hyderabad,
Hyderabad 500 046, India

Introduction

Much attention has been paid to microwave absorption materials due to their unique absorbing microwave energy and promising applications (Shin and Oh 1993; Martha 2000; Peng et al. 2005). Extensive study has been carried out to develop new microwave absorbing materials with a high magnetic and electric loss (Ruan et al. 2000; Babbar et al. 2000; Verma et al. 2003; Cho et al. 1996; Singh et al. 2000; Nakamura 2000). To our knowledge, ferrites might be a candidate as the microwave absorbing materials because of their high-specific resistance, remarkable flexibility in tailoring the magnetic properties and ease of preparation (Martha 2000). In the past decades, the spinel ferrites have been utilized as the most frequent absorbing materials in various forms (Peng et al. 2005). Cobalt ferrite ($CoFe_2O_4$) is a common spinel ferrite material and has been widely used in microwave applications. Recently, it has been shown that magnetic nano-composites are useful as microwave absorbing materials due to their advantages in respect to light weight, low cost, design flexibility, and microwave properties over pure ferrites (Singh et al. 2000; Kim et al. 1996). On the other hand, titanium dioxide (TiO_2) is an important inorganic semiconductor and has temperature and environmentally stable dielectric properties (Dervos et al. 2004).

In the present investigation, the nanocomposites of TiO_2–$CoFe_2O_4$ with different mol% of TiO_2 were prepared using microwave–hydrothermal (M-H) method. The advantage of M-H method is given elsewhere (Komarneni et al. 1996). The as-prepared powders were characterized using X-ray diffraction (XRD), transmission electron microscope (TEM) and fourier transform infrared spectroscopy (FTIR). The TiO_2–$CoFe_2O_4$ composite materials were sintered at 500 °C/30 min using microwave sintering method, which helps them to meet the need for low

temperature co-fired ceramics technology. The frequency dependence of complex permittivity and permeability of the present composites were studied in the range of 1 MHz–1.8 GHz and the obtained results were discussed in this paper.

Experimental method

In the present investigation, $x\mathrm{TiO_2} + (1 - x)\,\mathrm{CoFe_2O_4}$ composites ($0 \leq x \geq 1$) were prepared using appropriate amounts of TiO_2 and $CoFe_2O_4$ solutions. The $CoFe_2O_4$ was prepared using cobalt nitrate [$Co(NO_3)_2{\cdot}6H_2O$] and ferric nitrate [$Fe(NO_3)_2{\cdot}9H_2O$] in stoichiometric ratio. The TiO_2 was synthesized using titanium tetrachloride ($TiCl_4$) solutions. These reagents were dissolved in 50 ml of de-ionized water. To this solution, sodium hydroxide (NaOH) was added to maintain the pH of the solution ~12. Controlling of pH is the key factor to synthesize the nanopowder.

The $x\mathrm{TiO_2} + (1 - x)\,\mathrm{CoFe_2O_4}$ composite precipitation was transferred into double-walled digestion vessels that have an inner liner and cover made up of Teflon PFA and an outer high strength layer made up of Ultem polyetherimide and then treated using M-H method at 165 °C/45 min. The M-H treatment was performed using a microwave accelerated reaction system (MARS-5, CEM Corp., Mathews, NC, USA). This system uses 2.45 GHz microwave frequency and can be operated at 0–100 % full power (1,200 ± 50 W). The reaction vessel was connected to an optical probe to monitor and control the temperature during synthesis. The product was separated by centrifugation and then washed repeatedly with de-ionized water, followed by drying in an oven overnight at 100 °C. Thus, the obtained powders were weighed and the percentage yields were calculated from the total expected based on the solution concentration and volume and the amount that was actually crystallized. A 94 % of the yield was obtained. A similar procedure was followed to obtain different mol% of TiO_2 composites.

The phase identification of powders was performed using XRD with Cu K_α ($\lambda_{\mathrm{CuK}\alpha} = 1.54056$ Å) radiation. The particle size was calculated from TEM. The powders were uniaxially pressed into toroidal samples and pellets. The specimens were sintered at 500 °C/30 min using microwave sintering method (Murthy 2002). The microwave sintering process was carried out using a domestic microwave oven, operated at 2.45 GHz of frequency and an output power tunable up to 1,100 W. Temperature of the sample was measured using platinum sheathed Cr–Al thermocouple with an accuracy of ±1 °C. The temperature of the furnace was controlled with a PID controller. The sintering temperature was chosen for maximum ceramic density without apparent chemical reaction as determined from XRD analysis.

The phase identification and grain distribution of the sintered samples were identified using XRD and field emission scanning electron microscope (FE-SEM). The bulk density of the present samples was measured using the Archimedes principle. The frequency dependent complex permittivity (ε' and ε'') and permeability (μ' and μ'') were measured in the range of 1 MHz–1.8 GHz using Agilent 4291B impedance analyzer at room temperature.

Results and discussion

Figure 1 shows the XRD patterns of the as-synthesized powders of TiO_2 ($x = 1.0$), $CoFe_2O_4$ ($x = 0$) and $x\mathrm{TiO_2} + (1 - x)\,\mathrm{CoFe_2O_4}$ ($x = 0.9$–0.1) composite powders, respectively. It can be seen from the figure that the powders possess anatase phase ($x = 1$) (JCPDS card no. 89-4203) and spinel phase ($x = 0$) (JCPDS card no. 03-0864), respectively. It can be seen from the figure that both TiO_2 and ferrite peaks are present in the XRD patterns. No other phases were detected in the XRD patterns. The crystallite size (D_m) of the $CoFe_2O_4$ in the composite has been estimated with the help of (3 1 1) peak using Scherrer's equation: $D_m = K\lambda/\beta\cos\theta$, where K is a constant, β the full width half maxima, λ the wavelength of X-rays used and θ is the diffraction angle. The crystallite

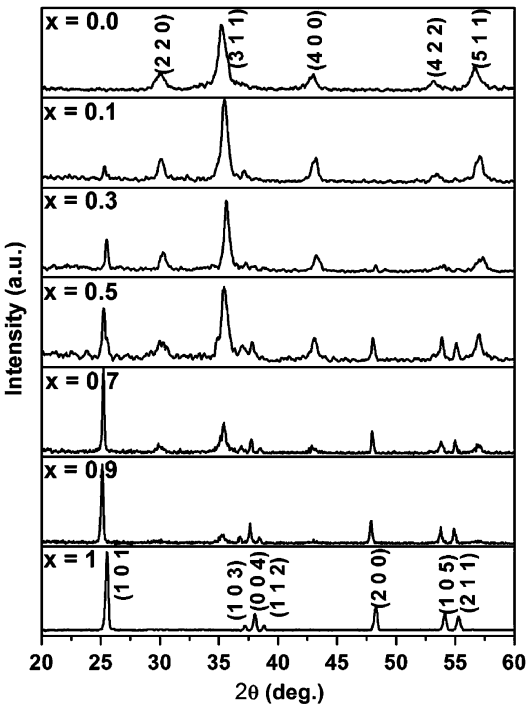

Fig. 1 XRD patterns of microwave–hydrothermally synthesized $x\mathrm{TiO_2} + (1 - x)\,\mathrm{CoFe_2O_4}$ composites ($0 \leq x \geq 1$)

Table 1 Data of lattice constant and crystallite size

Composition	Sample name	Lattice constant			Crystallite size of ferrite calculated from (3 1 1) peak (nm)
		Ferrite	TiO_2		
		(a) (Å)	(a) (Å)	(c) (Å)	
TiO_2	TO	–	3.701	9.499	–
0.9 mol% TiO_2 + 0.1 mol% $CoFe_2O_4$	CFT9	8.386	3.701	9.499	30
0.7 mol% TiO_2 + 0.3 mol% $CoFe_2O_4$	CFT7	8.382	3.701	9.502	26
0.5 mol% TiO_2 + 0.5 mol% $CoFe_2O_4$	CFT5	8.378	3.699	9.505	25
0.3 mol% TiO_2 + 0.7 mol% $CoFe_2O_4$	CFT3	8.372	3.699	9.505	23
0.1 mol% TiO_2 + 0.9 mol% $CoFe_2O_4$	CFT1	8.365	3.699	9.509	21
$CoFe_2O_4$	CF	8.361	–	–	20

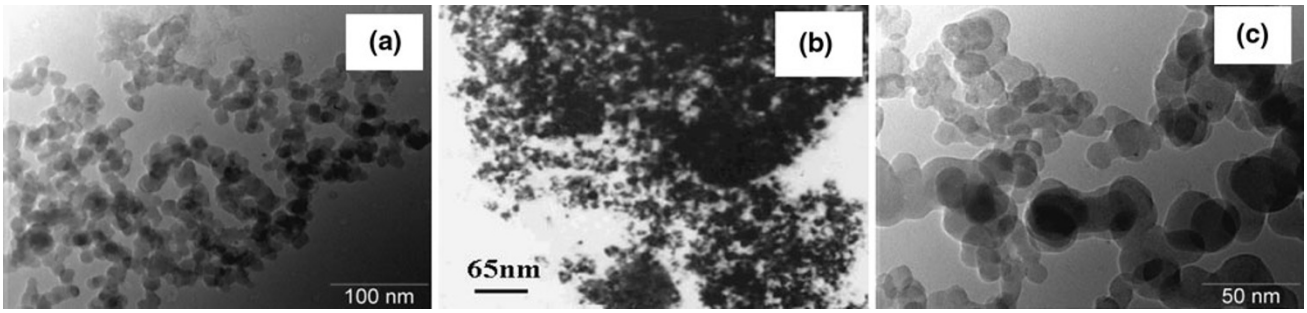

Fig. 2 TEM images of **a** TiO_2, **b** $CoFe_2O_4$ and **c** 50 wt% TiO_2 composite

sizes of the ferrite in the composite and lattice constants of the composites were given in Table 1. It can be seen from the table that the crystallite size decreases and lattice parameters increase with an increase of TiO_2 content.

Figure 2a, b and c shows the TEM pictures of the as-synthesized TiO_2, $CoFe_2O_4$ and 0.5 mol% TiO_2 + 0.5 mol% $CoFe_2O_4$ powders, respectively. From the TEM pictures, the average particle size was calculated and it was found to be ~18, 22 and ~24 nm for TiO_2, $CoFe_2O_4$ and 0.5 mol% TiO_2 + 0.5 mol% $CoFe_2O_4$ powders, respectively.

Figure 3a, b and c shows the FTIR spectra of as-synthesized $xTiO_2 + (1 - x)\,CoFe_2O_4$ $(0 \leq x \geq 1)$ composite powders. Figure 3a shows the FTIR spectra of as-synthesized TiO_2 powders. The broad absorption in the 3,600–2,800 cm^{-1} range, with a maximum at 3,486 cm^{-1}, arises from the stretching vibrations of O–H group (i.e., involved in hydrogen bonds) and the symmetric and anti-symmetric ν_{OH} modes of molecular water coordinated to Ti^{4+} cations (Morterra 1988; Primet et al. 1971). The band at 1,616 cm^{-1} is assigned to the molecular water bending mode. The band at 1,379 cm^{-1} is ascribed to the anti-symmetric stretching vibration of NO_3^{-1}, arising from the residual nitrate. The broad peak in the range of 800–500 cm^{-1} is identified to have the frequencies corresponding to bulk titania skeletal (Kumar et al. 2000).

Figure 3b shows the FTIR spectra of as-synthesized $CoFe_2O_4$ powders. It can be seen from the figure that there are two main broad, in the range of 400–300 cm^{-1} and 600–500 cm^{-1}, bands are observed. The highest one, ν_1, is generally observed in the range 600–500 cm^{-1}, and it corresponds to intrinsic stretching vibrations of the metal at the tetrahedral site (T_d), $M_{tetra} \leftrightarrow O$, whereas the ν_2, lowest band is usually observed in the range 430–385 cm^{-1}, is assigned to octahedral metal stretching (O_h), $M_{octa} \leftrightarrow O$ (Baykal et al. 2008; Patil et al. 1998). In the FTIR spectrum, the band at 579 cm^{-1} is assigned as ν_1 ($M_{tetra} \leftrightarrow O$) and 405 cm^{-1} is assigned as ν_2. The band at 975 cm^{-1} may be ascribed to the stretching vibration of Fe–Co. The absorption bands at 3,450 and 1,615 cm^{-1} arise from the stretching and bending vibrations of hydroxyl groups, respectively. The band at 1,379 cm^{-1} is ascribed to the anti-symmetric stretching vibration of NO_3^{-1}, arising from the residual nitrate.

Figure 3c shows the FTIR spectra of as-synthesized $xTiO_2 + (1 - x)\ CoFe_2O_4$ $(0.1 \leq x \geq 0.9)$ composite powders. The band at 375–800 cm^{-1} is attributed to the Ti–O–Ti or Fe–O stretching vibrations. It can be seen from the figure that as the mol% of TiO_2 is increasing, the intensity of the bands at 579 cm^{-1} increases and shifts towards high frequency. The band became broad at high

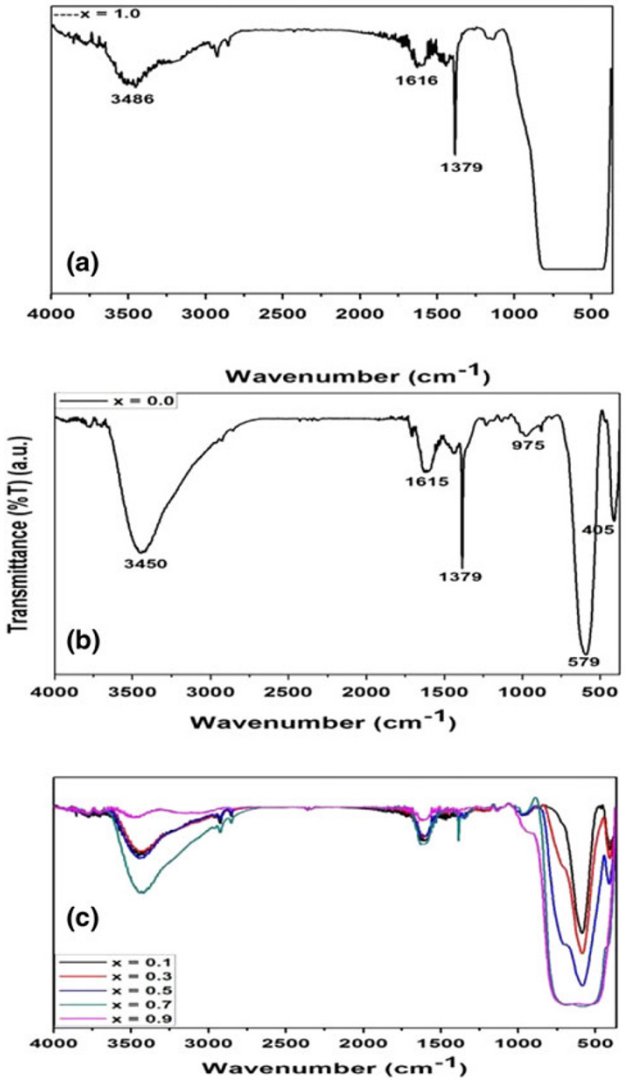

Fig. 3 FTIR spectra of microwave–hydrothermally synthesized **a** TiO_2, **b** $CoFe_2O_4$ and **c** $xTiO_2 + (1 - x)$ $CoFe_2O_4$ composites ($0.1 \leq x \geq 0.9$)

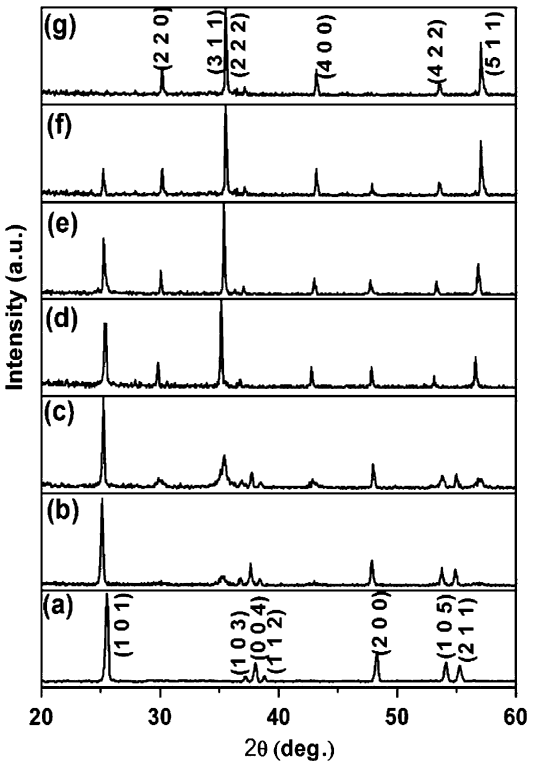

Fig. 4 XRD patterns of microwave sintered $xTiO_2 + (1 - x)$ $CoFe_2O_4$ composites ($0 \leq x \geq 1$). **a** TO, **b** CFT9, **c** CFT7, **d** CFT5, **e** CFT3, **f** CFT1 and **g** CF

mol% of TiO_2. The band at 405 cm^{-1} is disappearing when the mol% of TiO_2 is increasing, indicates that Ti^{4+} ions occupy octahedral sites of spinel structure.

Figure 4 shows the XRD patterns of nanocomposite samples sintered at 500 °C/30 min. It is clearly seen that two phases, ferrite and anatase, were identified in the composite samples. No intermediate phases such as $CoTiO_3$ (JCPDS card no: 72-1069) and Fe_2O_3 were observed in the X-ray analysis. This suggests that no significant chemical reactions were taken place during co-firing of the mixed powders, remaining the presence of distinct TiO_2 and ferrite phases. This is very important for the preparation of ferrite + TiO_2 composite materials, so that the dielectric properties of the composites could not degrade after sintering. It can also be observed that the number of ferrite peaks increases with an increase of ferrite content in the composite and vice versa. It clearly shows that the sintering at 500 °C/30 min enhanced the intensity of composite diffraction peaks which indicates the improvement of crystallizability. The lattice parameters of the composites were given in Table 2. It can be seen from the table that the lattice parameters were increasing with an increase of TiO_2 content.

At 500 °C, Ti^{4+} (1.34 Å) substitute the Fe^{3+} ion (0.64 Å) at A and B sites of the spinel ferrite structure, according to the law of ion substitution. Ti^{4+} ions occupy the B sites of spinel ferrite structure; due to this, the lattice constant increases with an increase of TiO_2 content. The lattice parameter of the TiO_2 is not changed uniformly. The bulk density of the present sintered samples was measured using Archimedes's method and it was found to be increasing with an addition of TiO_2.

Figure 5a–d shows the FE-SEM images of the composites with different mol% of TiO_2. The microstructure properties like grain size, grain distribution and porosity significantly influence the properties of the composite materials. It is therefore essential to have a detailed microstructure analysis. In the images, the black grains are ferrite grains and the white ones are TiO_2 grains. The values of grain sizes of ferrite were given in Table 2. It can be observed from the images that the grain size is in the range of 54–78 nm. It can be seen that as

Table 2 Data of lattice constant, bulk density, M_s and dielectric and magnetic properties of sintered samples

Sample name	Lattice constant			Bulk density (g/cm^3)	Grain size of the ferrite (nm)	M_s (emu/g)	At 1 MHz			
	Ferrite	TiO_2					ε'	ε''	μ'	μ''
	(a) (Å)	(a) (Å)	(c) (Å)							
TO	–	3.773	9.509	–	–	–	–	–	–	–
CFT9	8.399	3.773	9.509	5.45	78	–	44	2.46	32	1.35
CFT7	8.397	3.773	9.511	5.42	72	–	36	2.21	71	1.67
CFT5	8.395	3.774	9.512	5.39	66	4	30	2.16	110	1.98
CFT3	8.394	3.774	9.512	5.35	60	10	24	1.85	172	2.27
CFT1	8.394	3.774	9.514	5.33	54	22	19	1.46	398	2.52
CF	8.393	–	–	5.30	–	34	14	1.12	773	2.84

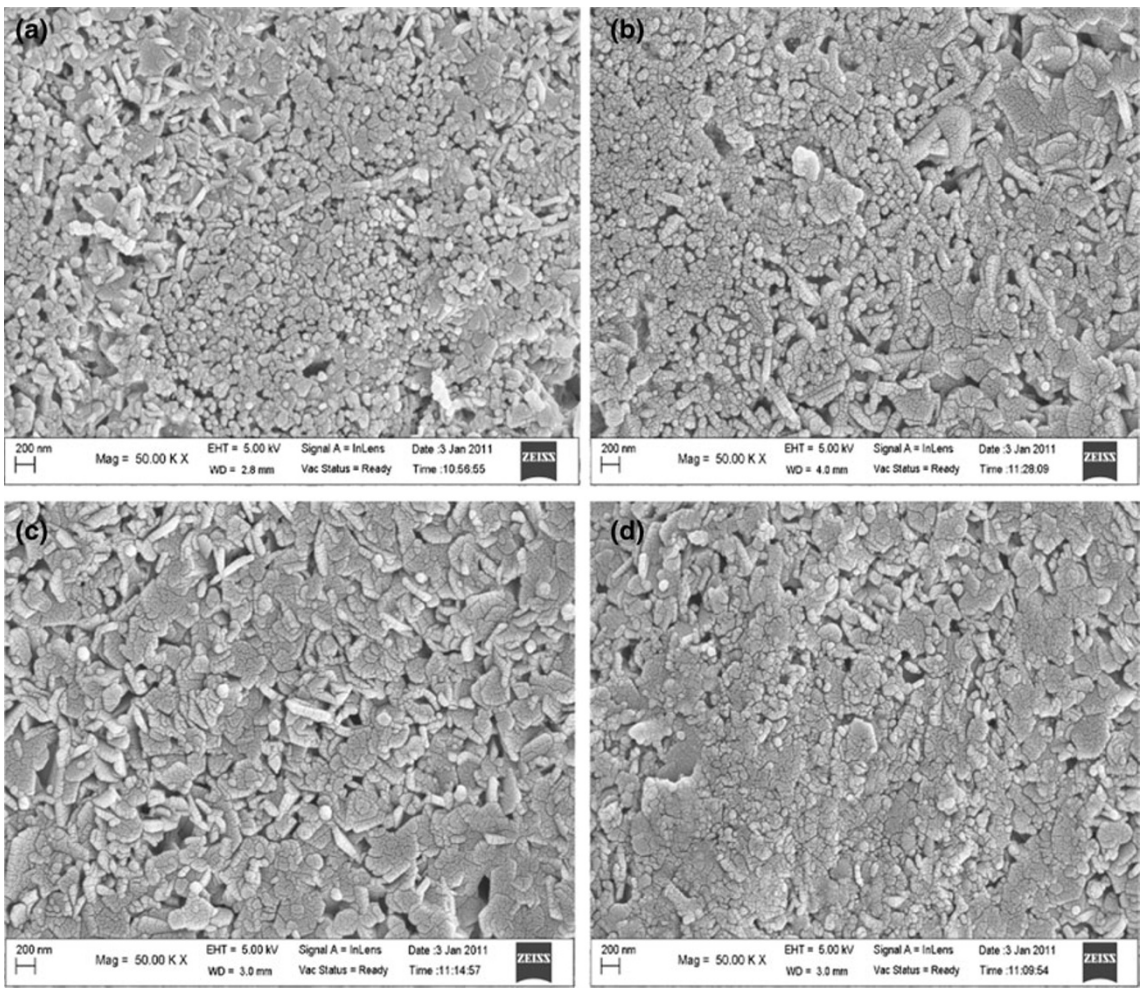

Fig. 5 SEM images of microwave sintered $xTiO_2 + (1 - x)\ CoFe_2O_4$ composites ($0 \leq x \geq 1$). **a** CFT3, **b** CFT5, **c** CFT7 and **d** CFT9

the TiO_2 content increasing, the samples are becoming dense. The sample CFT9 shows less pores and the distribution of the grains is uniform.

Figure 6 shows the magnetic hysteresis loops of $xTiO_2 + (1 - x)\ CoFe_2O_4$ nanocomposites with $x = 0$, 0.1, 0.3, 0.5 and 0.7 mol%, respectively, indicating that the composites are magnetically ordered. The values of saturation magnetization (M_s) were given in Table 2. It is observed that the values of saturation magnetization of the composites were found to be decreasing with an increase of

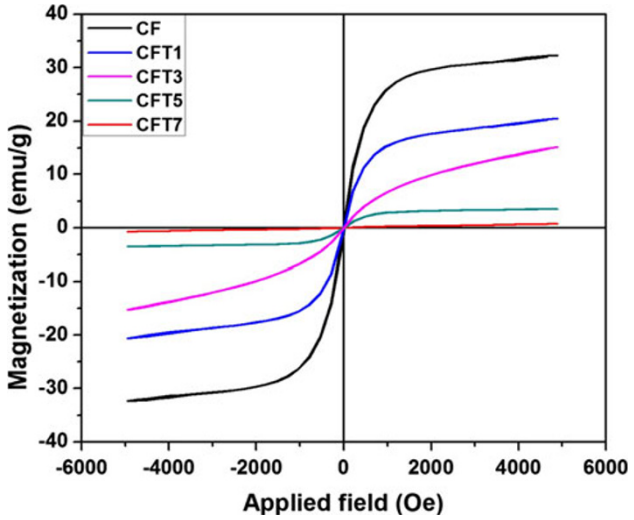

Fig. 6 VSM loops of $TiO_2 + CoFe_2O_4$ nanocomposites

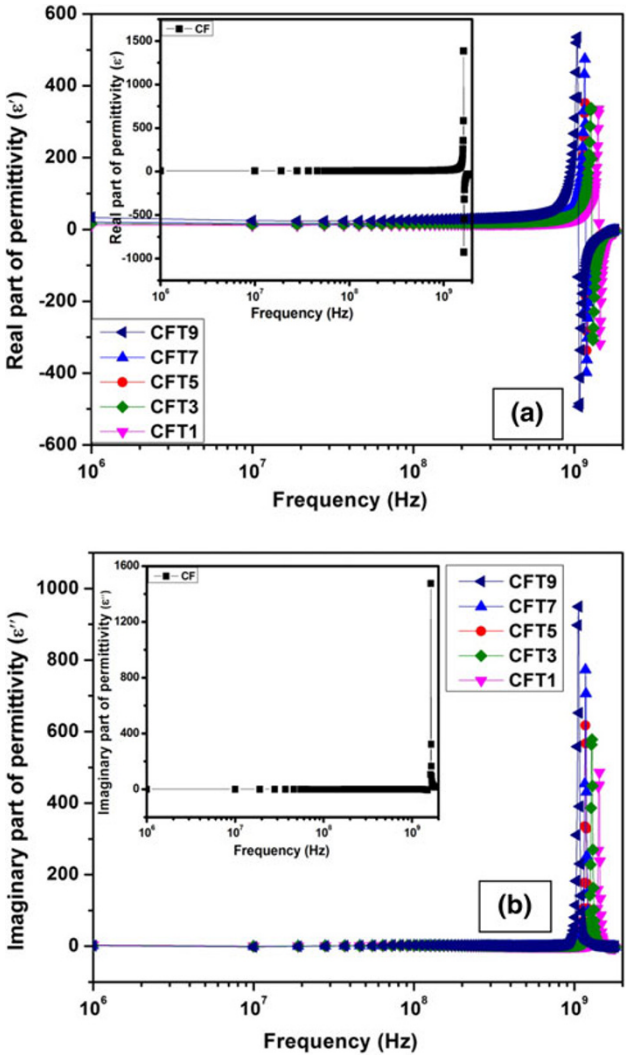

Fig. 7 Frequency dependence of **a** real (ε') and **b** imaginary (ε'') parts of permittivity

TiO_2 due to the dilution effect of non-magnetic TiO_2. The saturation magnetization of TiO_2 is unity due to its inherent non-magnetic nature.

The frequency variation of real (ε') and imaginary (ε'') parts of permittivity for all the samples under investigation was measured in the frequency range of 1 MHz–1.8 GHz and obtained results are plotted in Fig. 7a and b. It can be seen from the figures that the value of ε' remains constant up to 300 MHz and increases further increase of frequency. In all the samples, a resonance peak was observed around 1 GHz. This behavior can be explained in the following way: the ε' remains constant in the frequency range from 1 to 300 MHz due to the hoping electrons will not follow the external applied field. Whereas, the increase of ε' around 1 GHz is may be due to the following of hopping electrons with the external field. When the hoping frequency of the electrons is equal to that of the external applied electric field, a peak obtained is called as the dielectric resonance.

As TiO_2 increases from $x = 0.1$ to 0.9, the values of ε' also increases from 19 to 44 at 1 MHz and the values were given in Table 2. The increase of real part of permittivity (ε') is attributed to the introduction of TiO_2 which raises the amount of dipoles in the composite materials. The increase of dipoles tends to increase the local displacements (dielectric polarization) in the direction of external applied electric field for electrons, and the increased polarization causes a significant enhancement of the dielectric constant. The frequency dependence of imaginary part of permittivity (ε'') has been measured on all the composites in the range of 1 MHz–1.8 GHz and obtained results were plotted in Fig. 7b. It can be seen from the figure that the value of ε' is small and remains almost constant from 1 to 300 MHz. The ε'' value increases with an increase of TiO_2 content. The variation of ε'' with frequency may be explained similar to that of ε' variation with frequency. The change in the ε' and ε'' with frequency for TiO_2–$CoFe_2O_4$ composites obeys Lichtenecker's mixed law (Kondo et al. 1999).

Figure 8 shows the frequency dependence of complex permeability for composite samples at room temperature. It was observed from the figures that the real (μ') part of permeability remained almost constant, until the frequency was raised to a certain value and then began to decrease at higher frequency. The imaginary (μ'') part of permeability gradually increased with the frequency and took a maximum at a certain frequency, where the μ' rapidly decreases. This feature is well known as natural resonance. As the wt% of TiO_2 increases from $x = 0.1$ to 0.9, the real part of permeability (μ') decreases to very small value at 1 MHz, and the values were given in Table 2. It can be observed from the figure that the magnetic resonance frequency for the composite increases with decrease in ferrite content.

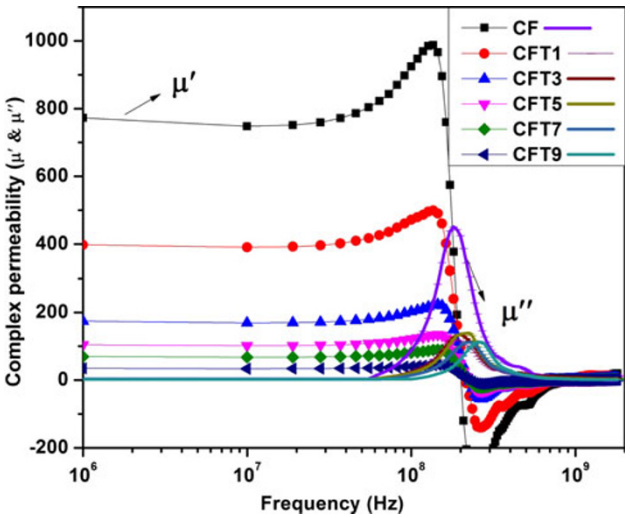

Fig. 8 Frequency dependence of real (μ') and imaginary (μ'') parts of permeability

This may be attributed to the decrease in the interaction between ferrite particles due to the dilute effect of non-magnetic particles. With an increase of TiO_2, the natural resonance frequency having a maximum value shifted towards high frequency.

The μ'' of $TiO_2 + CoFe_2O_4$ composites are higher than that of pure $CoFe_2O_4$ in the whole frequency range. The result can be explained by magnetic dissipation. According to Van der Zaag's suggestion (Van der Zaag 1999), the magnetic dissipation of ferrites can be classified as: hysteresis loss, eddy current loss, residual loss, ferromagnetic resonance loss and intragranular domain wall loss. In this study, however, the enhancement of eddy loss might be contributed to higher μ'' of $TiO_2 + CoFe_2O_4$ nanocomposites, because of TiO_2 being a semiconductor with band gap energy of 3.2 eV (Zuo and Victoria 2003; Lee et al. 2004). Especially, when the weight ratio of TiO_2 is 20 %, both μ' and μ'' of $TiO_2 + CoFe_2O_4$ nanocomposites show maximum value.

Conclusions

For the first time $xTiO_2 + (1 - x)\ CoFe_2O_4$ nanocomposites were synthesized using microwave–hydrothermal method. The XRD shows the single phase formation of spinel and TiO_2 phases, respectively. High dense, homogeneous and small grained $CoFe_2O_4 + TiO_2$ were prepared using microwave sintering method at 500 °C/30 min. The variation of lattice constant was explained using structural formula. The average grain size of all the composites lies between 54 and 78 nm. The real permittivity and permeability values were not much affected by the addition of TiO_2 content, but the resonant frequency of all the sintered samples found to be >1 GHz.

Acknowledgments The authors K. Sadhana and K. Praveena are thankful to CSIR, New Delhi, India for providing Research Associate fellowship and to carry out the present work.

References

Babbar VK, Razdan A, Puri RA, Goel TC (2000) Complex permittivity, permeability, and X-band microwave absorption of CaCoTi ferrite composites. J Appl Phys 87:4362–4366

Baykal A, Kasapoglu N, Koseoglu Y, Basaran YC, Kavas H, Toprak MS (2008) Microwave-induced combustion synthesis and characterization of $Ni_xCo_{1-x}Fe_2O_4$ nanocrystals ($x = 0.0, 0.4, 0.6, 0.8, 1.0$). Eur J Chem 6(1):125–130

Cho SB, Kang DH, Oh JH (1996) Relationship between magnetic properties and microwave-absorbing characteristics of NiZnCo ferrite composites. J Mater Sci 31:4719–4722

Dervos CT, Thirios E, Novacovich P, Vassiliou P, Skafidas P (2004) Permittivity properties of thermally treated TiO_2. Mater Lett 58:1502–1507

Kim DY, Chung YC, Kang TW, Kim HC (1996) Dependence of microwave absorbing property on ferrite volume fraction in MnZn ferrite–rubber composites. IEEE Trans Magn 32:555–558

Komarneni S, Menon VC, Roy R, Li QH, Ainger F (1996) Microwave–hydrothermal processing of $BiFeO_3$ and $CsAl_2PO_6$. J Am Ceram Soc 79(5):1409–1412

Kondo T, Aoki T, Asano K, Yoshikado S (1999) Fabrication of the composite electromagnetic wave absorber, IEEE EMC Symposium, pp 397–400

Kumar PM, Badrinarayanan S, Sastry M (2000) Nanocrystalline TiO_2 studied by optical, FTIR and X-ray photoelectron spectroscopy: correlation to presence of surface states. Thin Solid Films 358:122–130

Lee DK, Kim SC, Kim SJ, Chung SI, Kim SW (2004) Photocatalytic oxidation of microcystin-LR with TiO_2-coated activated carbon. Chem Eng J 102:93–98

Martha PH (2000) Microwave applications of soft ferrites. J Magn Magn Mater 215–216:171–183

Morterra C (1988) An infrared spectroscopic study of anatase properties. Part 6. Surface hydration and strong Lewis acidity of pure and sulphate-doped preparations. J Chem Soc Faraday Trans 84:1617–1637

Murthy SR (2002) Low temperature sintering of NiCuZn ferrite and its electrical, magnetic and elastic properties. J Mat Sci Letters 21(8):657–660

Nakamura T (2000) Snoek's limit in high-frequency permeability of polycrystalline Ni–Zn, Mg–Zn, and Ni–Zn–Cu spinel ferrites. J Appl Phys 88:348–353

Patil SA, Mahajan VC, Ghatage AK, Lotke SD (1998) Structure and magnetic properties of Cd and Ti/Si substituted cobalt ferrites. Mater Chem Phys 57:86–91

Peng CH, Hwang CC, Wan J, Tsai JS, Chen SY (2005) Microwave absorbing characteristics for the composites of thermal-plastic polyurethane (TPU)-bonded NiZn-ferrites prepared by combustion synthesis method. Mater Sci Eng B 117:27–36

Primet M, Pichat P, Mathieu MV (1971) Infrared study of the surface of titanium dioxides. I. Hydroxyl groups. J Phys Chem 75(9):1216–1220

Ruan S, Xu B, Suo H, Wu F, Xiang S, Zhao M (2000) Microwave absorptive behavior of ZnCo-substituted W-type Ba hexaferrite

nanocrystalline composite material. J Magn Magn Mater 212:175–177

Shin JY, Oh JH (1993) The microwave absorbing phenomena of ferrite microwave absorbers. IEEE Trans Magn 29:3437–3439

Singh P, Babbar VK, Razdan A, Srivastava SL, Goel TC (2000) Microwave absorption studies of Ca–NiTi hexaferrite composites in X-band. Mater Sci Eng B 78:70–74

Vander Zaag PJ (1999) New views on the dissipation in soft magnetic ferrites. J Magn Magn Mater 196–197:315–319

Verma A, Saxena AK, Dube DC (2003) Microwave permittivity and permeability of ferrite–polymer thick films. J Magn Magn Mater 263:228–234

Zuo X, Victoria C (2003) Calculation of exchange integrals and electronic structure of manganese ferrite ($MnFe_2O_4$). J Appl Phys 93:8017–8019